Title
Regulation of the formin cappuccino is critical for polarity of Drosophila oocytes

Journal
Cytoskeleton, 72(1)

ISSN
1949-3584

Authors
Bor, Batbileg
Bois, Justin S
Quinlan, Margot E

Publication Date
2015

DOI
10.1002/cm.21205

Peer reviewed

Published in final edited form as:

Cytoskeleton (Hoboken). 2015 January ; 72(1): 1–15. doi:10.1002/cm.21205.

Regulation of the formin Cappuccino is critical for polarity of *Drosophila* oocytes

Batbileg Bor[1], **Justin S. Bois**[2,3], and **Margot E. Quinlan**[2,4,*]

[1]Molecular Biology Interdepartmental PhD Program, University of California, Los Angeles, CA 90095-1570

[2]Department of Chemistry and Biochemistry, University of California, Los Angeles, CA 90095-1570

[4]Molecular Biology Institute, University of California, Los Angeles, CA 90095-1570

Abstract

The *Drosophila* formin Cappuccino (Capu) creates an actin mesh-like structure that traverses the oocyte during mid-oogenesis. This mesh is thought to prevent premature onset of fast cytoplasmic streaming which normally happens during late-oogenesis. Proper cytoskeletal organization and cytoplasmic streaming are crucial for localization of polarity determinants such as *osk*, *grk*, *bcd* and *nanos* mRNAs. Capu mutants disrupt these events, leading to female sterility. Capu is regulated by another nucleator, Spire, as well as by autoinhibition *in vitro*. Studies *in vivo* confirm that Spire modulates Capu's function in oocytes; however, how autoinhibition contributes is still unclear. To study the role of autoinhibition in flies, we expressed a Capu construct that is missing the Capu Inhibitory Domain, CapuΔN. Consistent with a gain of activity due to loss of autoinhibition, the actin mesh was denser in CapuΔN oocytes. Further, cytoplasmic streaming was delayed and fertility levels decreased. Localization of *osk* mRNA in early stages, and *bcd* and *nanos* in late stages, were disrupted in CapuΔN-expressing oocytes. Finally, evidence that these phenotypes were due to a loss of autoinhibition comes from co-expression of the N-terminal half of Capu with CapuΔN, which suppressed the defects in actin, cytoplasmic streaming and fertility. From these results, we conclude that Capu can be autoinhibited during *Drosophila* oocyte development.

Keywords

Capu; actin; mRNA; autoinhibition; polarity

*Correspondence should be addressed to M.E.Q. (margot@chem.ucla.edu).

[3]Current address for JSB: Division of Biology and Biological Engineering, California Institute of Technology, MC 114-96, Pasadena, CA 91125

Competing interests statement

The authors declare no competing financial interests.

Introduction

Cappuccino (Capu) was originally identified in a screen for maternal-effect genes important for pattern formation. Mutations in *capu* disrupt both anteroposterior (AP) and dorsoventral (DV) axis formation of the *Drosophila* embryo, resulting in female sterility [Manseau and Schüpbach, 1989]. The original studies of *capu* led to the hypothesis that this gene, along with a second gene, *spire*, contributed to both major body axes by localizing and/or stabilizing other patterning factors by regulating the cytoskeleton [Manseau and Schüpbach, 1989; Emmons et al., 1995].

Detailed biochemical and genetic analysis of Capu support this hypothesis and shed light on how Capu regulates polarity. Capu is a member of the formin family of actin nucleators [Emmons et al., 1995]. As such, it has well-conserved formin homology 1 and 2 (FH1 and FH2) domains in its C-terminal half [Higgs and Peterson, 2005]. FH2 domains are crucial for actin filament nucleation and remain associated with the barbed ends of growing filaments to control elongation [Higashida et al., 2004; Otomo et al., 2005; Pruyne et al., 2002]. FH1 domains bind to profilin-actin to facilitate fast delivery of actin monomers to the FH2 bound barbed ends [Paul et al., 2008]. Consistent with Capu's actin polymerization activity, recently, Capu was linked to two actin structures in *Drosophila* oocytes: an isotropic mesh that traverses the oocyte cytoplasm, which is present throughout mid-oogenesis (stages 5-10), and a network of long filaments extending from the posterior cortex of the oocyte present at later stages [Chang et al., 2011; Dahlgaard et al., 2007; Tanaka et al., 2011].

A dramatic change in ooplasm dynamics coincides with disappearance of the actin mesh at stage 10B. At early stages, the fluid within the oocyte moves in a slow, uncoordinated manner. After stage 10B, this fluid flow is ~10 times faster and coordinated [Gutzeit and Koppa, 1982; Serbus et al., 2005]. At this time microtubules reorganize from a biased random anterior-posterior polarity to parallel bundles along the oocyte cortex [Parton et al., 2011; Theurkauf et al., 1992]. *capu* mutants exhibit premature onset of cytoplasmic streaming [Theurkauf, 1994]. Multiple studies link the Capu-dependent actin mesh to control of the timing of cytoplasmic streaming [Dahlgaard et al., 2007; Quinlan, 2013].

Establishment of the major body axes in *Drosophila* oocytes requires proper localization of polarity determinants such as *gurken* (*grk*), *oskar* (*osk*), *bicoid* (*bcd*) and *nanos* mRNAs [Frohnhöfer and Nüsslein-Volhard, 1986; Lehmann and Nüsslein-Volhard, 1986; Lehmann and Nüsslein-Volhard, 1991; Schüpbach, 1987; Wang and Lehmann, 1991]. Localization of these polarity determinants is largely dependent on microtubules and their associated motors, while both actin and microtubules are required for anchoring. Modes of transport and anchoring are specific to each polarity factor and the stage of development. For example, *osk*, which is enriched at the posterior after stage 7, is transported by kinesin along microtubules which are oriented with a slight bias towards the posterior at this time [Brendza et al., 2000; Ephrussi et al., 1991; Kim-Ha et al., 1991; Parton et al., 2011; Zimyanin et al., 2007]. In contrast, the majority of *nanos* is localized to the posterior after stage 10 by a combination of advection due to cytoplasmic streaming and entrapment at the

posterior, as opposed to active transport by a motor [Wang et al., 1994; Forrest and Gavis, 2003].

grk, *osk* and *nanos*, but not *bcd*, localizations are disrupted in *capu* mutants [Ephrussi et al., 1991; Manseau et al., 1996; Neuman-Silberberg and Schüpbach, 1993; Wang et al., 1994]. Premature cytoplasmic streaming in *capu* mutants could mechanically disrupt the mRNA localization, or subsequent reorganization of the microtubule cytoskeleton may prevent the correct localization of mRNAs [Theurkauf, 1994]. Given that these factors continue to accrue correctly after normal cytoplasmic streaming begins, it is not obvious why premature streaming is so detrimental. Perhaps establishment of "landing sites" is more delicate than later delivery of polarity factors. *Osk* at least has a positive feedback mechanism whereby the anchoring site at the posterior has to be established at early stages. Once established, more *osk* can be recruited during later stages [Sinsimer et al., 2011; Snee et al., 2007]. How *capu* contributes to the second step of mRNA localization is also unclear. It may be that Capu-dependent posterior filaments detected later in oogenesis are necessary for anchoring/entrapment during both early and late phases of mRNA transport.

Capu, like any actin nucleator, needs to be regulated. Until recently, Spire was the sole candidate for modulating Capu's functions [Quinlan, 2013; Quinlan et al., 2007]. However, we found that Capu can also be autoinhibited, like most other formins [Bor et al., 2012]. We identified an N-terminal Capu Inhibitory Domain (CID; Capu1-222) that binds the C-terminal Capu-tail domain to inhibit Capu's polymerization and elongation activities. This raises the question of how Capu is regulated during *Drosophila* oogenesis. Several lines of evidence support a role for Capu autoinhibition: replacement of endogenous Capu with a version lacking the first 270 residues (green fluorescent protein [GFP]-CapuΔN) induced an actin mesh in the nurse cells and oocyte [Dahlgaard et al., 2007]; Capu's N-terminal 100 amino acids exert a dominant-negative effect on Capu's oskar protein-anchoring activity, possibly by inhibiting formation of the actin filaments extending from the posterior cortex [Chang et al., 2011]. Despite these observations, it is still unclear how Capu is regulated during oocyte development. We therefore further characterized Capu autoinhibition during *Drosophila* oogenesis by expressing the N-terminal half of Capu, which contains the CID domain (CapuNT), and truncated Capu that is lacking the CID domain (CapuΔN) in a wild type background. Overexpression of constitutively active Capu caused fertility defects. These oocytes had increased actin mesh density that persisted beyond stage 11 and inhibited cytoplasmic streaming. Furthermore, we observed that *osk* was not correctly localized during early stages and *bcd* and *nanos* failed to localize or localized at lower levels than wild type during late stages of oogenesis. By coexpressing CapuNT, we were able to rescue the fertility, actin mesh, and cytoplasmic streaming phenotypes, suggesting that Capu is regulated by autoinhibition *in vivo*. Therefore, we find that not only can Capu be autoinhibited in *Drosophila* oocytes, but properly regulated actin mesh and cytoplasmic streaming are critical for localization of polarity determinants and fertility.

Results

Constitutively active Capu decreases fertility

Previously, we demonstrated that Capu is autoinhibited *in vitro* [Bor et al., 2012]. To test whether autoinhibition is important during *Drosophila* oogenesis, we expressed a form of Capu believed to be constitutively active, GFP-CapuΔN, in wild type background and assessed its effect on fertility (Figure 1A, B). We used two different germline-specific drivers to express GFP-CapuΔN: the maternal α-tubulin promoter (*matα*-Gal4-VP16; *matα*) and the *nanos* promoter (*nos*-Gal4-VP16; *nos*). *matα* is a strong driver throughout oogenesis. In contrast, *nos* drives expression in the germarium, and again after stage 8 with low expression between stages 3-8 [Hudson and Cooley, 2010]. Based on the consistent and strong expression, we used the *matα* driver in all of our experiments. We also compared our results to those with the *nos* driver where possible. For comparison, we expressed full-length Capu (GFP-CapuFL), and GFP alone. We measured fertility rates of female flies by crossing them to wild type males, collecting eggs and counting the number that hatched within 24 hours. When we used the *nos* driver, only 48% of eggs hatched when laid by flies expressing GFP-CapuΔN (*nos*:GFP-CapuΔN; Figure 1B). In contrast, 89% of eggs hatched from flies expressing GFP-CapuFL (*nos*:GFP-CapuFL). When we used the *matα* driver, we saw enhanced fertility defects for both GFP-CapuΔN (17%; *matα*:GFP-CapuΔN) and GFP-CapuFL (52%; *matα*:GFP-CapuFL) (Figure 1B). To understand why *matα*:GFP-CapuFL was so detrimental, we tested the effect of expressing unlabeled CapuFL or GFP alone. Consistent with the difference in drivers, *matα* driven expression of GFP (*matα*:GFP) also compromised fertility (73% hatched) as compared to the effect of *nos* driven expression (*nos*:GFP), which was negligible (93%) (Figure 1B). We believe this loss in fertility is due to a combination of expressing large amounts of GFP as well as Gal4 since *matα* flies are generally sicker than wild type. CapuFL expression led to slightly increased fertility compared to GFP-CapuFL expression in *matα* flies (59% vs. 52%, data not shown). This observation is consistent with data from Dahlgaard et al. [2007] which indicate that the GFP tag increases Capu activity [Dahlgaard et al., 2007]. It also confirms that overexpression of CapuFL impacts fertility. We interpret the fertility defects of both GFP-CapuΔN and GFP-CapuFL as a consequence of overactive Capu, with the strongest defects caused by the constitutively active GFP-CapuΔN (Figure 1B).

Closer examination of the eggs laid in these experiments revealed that expression of GFP-CapuΔN caused polarity defects similar to those described for *capu* mutants. About 5% of *matα*:GFP-CapuΔN eggs had fused dorsal appendages (28/613) whereas *matα*:GFP-CapuFL had fewer such eggs (8/910). Fused dorsal appendages are a hallmark of defects in DV axis formation and appear in about 10% of strong *capu* alleles [Manseau and Schüpbach, 1989]. Further *matα*:GFP-CapuΔN embryos had disrupted abdominal segmentation, often lacked thoracic segments and displayed reduced head structures, which are hallmarks of defects in AP axis formation (Figure 1C). Interestingly, while *capu* mutants have AP defects, their embryos usually have abdominal segmentation defects but relatively normal thoraces and heads [Manseau and Schüpbach, 1989]. We draw two main conclusions from these experiments. First, an increase in Capu protein negatively impacts fertility and polarity. Second, truncating the CID domain (first 270 residues) enhances this negative effect. We

believe that these negative effects are due to an increase in Capu activity. However, based on these observations alone, we cannot rule out the possibility that truncation of the CID domain affects fertility and polarity through another mechanism.

GFP-CapuΔN expression leads to increased actin mesh density

We studied the actin mesh in the oocyte as a measure of Capu activity. Spire and Capu cooperate to build this structure [Dahlgaard et al., 2007; Quinlan, 2013]. In wild type oocytes, the mesh is present until stage 10, and it disappears by stage 11 (Figure S1A). We measured mesh density at stage 9, when the mesh is normally present, and stage 11, when it is normally absent. Again, we used *matα* and *nos* drivers to express GFP, GFP-CapuFL, or GFP-CapuΔN and compared these oocytes to those from wild type flies. The mesh in stage 9 oocytes was denser than wild type controls in both *matα*:GFP-CapuFL (2.3-fold) and *matα*:GFP-CapuΔN (2.9-fold) oocytes (Figure 2B, C, M and Table I). Further, while the absolute difference was not great, the mesh of *matα*:GFP-CapuΔN oocytes was significantly denser than that of *matα*:GFP-CapuFL oocytes. We note that at stage 9 the mesh density was also increased when GFP alone was expressed. The difference was small (1.4-fold compared to wild type oocytes) but statistically significant ($p < 0.03$) (Figure 2A and M). At stage 11, GFP expression had no effect on mesh density (Figure 2G and N). The mesh was absent, as expected. The mesh was denser when either *matα*:GFP-CapuFL (3.3-fold) or *matα*:GFP-CapuΔN (3.8-fold) were expressed (Figure 2H, I, N and Table I). At this stage, the difference between GFP-CapuFL and GFP-CapuΔN was not statistically significant, however. We note that the variance of mesh densities was higher at stage 11 and propose that the mesh density, which is normally zero, is more sensitive to Capu expression levels at this stage. We cannot distinguish whether the fertility defects are due to an increase in mesh density at stage 9, the presence of mesh at stage 11, or both. Regardless, these results support our hypothesis that there is a link between fertility phenotypes and an increase in Capu activity. Furthermore, GFP-CapuΔN is more active than GFP-CapuFL, probably due to loss of autoinhibition.

Supporting the idea that the level of actin mesh regulates fertility, *nos*-driven expression resulted in sparse mesh in comparison with the *matα* driver. While the overall impact was smaller the trends were the same: The mesh density increased at stage 9 of both *nos*:GFP-CapuFL (1.8-fold compared to GFP control) and *nos*:GFP-CapuΔN (2.2-fold) oocytes (Figure S2A-D and Table I). Stage 11 mesh density also increased (Figure S2E-H and Table I) for both *nos*:GFP-CapuFL (1.8-fold) and *nos*:GFP-CapuΔN (2.5-fold). At both stages 9 and 11, *nos*:GFP-CapuΔN resulted in significantly denser actin mesh than *nos*:GFP-CapuFL. The fact that *nos*:GFP-CapuFL causes an increase in mesh density at both stage 9 and 11 but has little effect on fertility suggests that the oocyte is resistant to an increase in mesh density. Increasing the mesh density beyond some threshold appears to negatively effect oocyte development because *nos*:GFP-CapuΔN had even higher mesh density both at stage 9 and 11 compared to *nos*:GFP-CapuFL, and this dense mesh corresponds to a dramatic decrease in fertility (Figure 1B and Table I).

When the actin mesh density was increased by *matα*:GFP-CapuΔN, we also observed other actin phenotypes. Similar to what was reported by Dahlgaard *et al*., stage 9 and 11 nurse

cells had actin mesh-like structures in their cytoplasm (Figure 2C, I). We also see actin mesh in GFP-CapuFL expressing nurse cells. This is consistent with our observation that GFP-CapuFL increased the mesh density in oocytes and the report that GFP partially activates CapuFL [Dahlgaard et al., 2007]. Therefore, we asked whether Capu activity affected additional aspects of oocyte development. The oocyte nucleus translates to the anterior-dorsal corner at stage 6-7. An increase in the oocyte actin mesh density did not disrupt this localization (Figure S1B and D), suggesting that the mesh dynamics are not altered, despite the increase in Capu's activity. Because the nucleus is much larger than the pore size of the actin mesh, its movement across the oocyte requires assembly and disassembly of the mesh in order to move significant distances. Because the nucleus moves from the posterior to the anterior-dorsal corner at the expected stage, we conclude that the rates of assembly and disassembly of the actin mesh are not slowed. We observed no change in border cell migration; border cells were found at the anterior of oocytes by stage 9 (Figure S1B and C). Nurse cell dumping relies on an actomyosin contraction. While an ectopic actin mesh in the nurse cells could disrupt this process by a number of mechanisms, dumping was apparently normal in GFP-CapuΔN and GFP-CapuFL flies. However, because fast streaming was prevented by the persistent actin mesh, we often saw that the oocyte contents were not mixed with the nurse cell contents, resulting in two layers of cytoplasm, as reported for expression of GFP-SpirD or loss of *khc* activity [Figure S1D; Dahlgaard et al., 2007; Palacios and St. Johnston, 2002; Serbus et al., 2005]. Therefore, we hypothesize that the increase in oocyte actin mesh density is the major cause of infertility.

Increased actin mesh density prevents late stage cytoplasmic streaming

In wild type oocytes, fluid flows are relatively slow while the actin mesh is present. Coinciding with the disappearance of the mesh at stage 10B, cytoplasmic streaming begins and by stage 11, this streaming is coordinated and about 10-times faster [Quinlan, 2013]. The cytoplasmic flow is readily visualized by imaging autofluorescent yolk granules. Using Particle Image Velocimetry (see methods), we quantified the velocity of cytoplasmic streaming in oocytes expressing GFP, GFP-CapuFL or GFP-CapuΔN at stages 9 and 11. Interestingly, despite the increase in actin mesh density, whether we used the *nos* or *matα* driver, these proteins had no effect on the motion in stage 9 oocytes (Figure 3A-C, M, S3A-D, and Table I). In contrast, the rate of cytoplasmic streaming at stage 11 was significantly lower (Figure 3G-I, N, S3E-H, and Table I). The average streaming velocity was low for *matα*:GFP-CapuFL (0.11 μm/s) and reduced to a rate similar to stage 9 for *matα*:GFP-CapuΔN (0.04 μm/s) (Figure 3G-I and N). This is consistent with the increase in actin mesh densities with *matα*-driven expression at stage 11 (Figure 2N). When we compare cytoplasmic streaming of *matα*:GFP-CapuFL to *matα*:GFP-CapuΔN, we also see significantly different speeds, consistent with the fertility results. At stage 11, *nos*:GFP-CapuFL (0.29 ± 0.12 μm/s) resulted in oocytes with the same velocity on average as *nos*:GFP (0.29 ± 0.07 μm/s) but the range of velocities was much broader, as reflected in the standard deviations (Figure S3E, F and H). Streaming was inhibited in most of the *nos*:GFP-CapuΔN oocytes (0.15 μm/s) (Figure S3G and H). The effect of the *matα* driver on streaming is more severe compared to the *nos* driver, consistent with this being a stronger driver overall. These data correlate with the increase in actin mesh described above. They suggest that an increase in Capu activity, due to increased protein level and/or truncating the

CID domain, inhibits cytoplasmic streaming during late stages, reflecting the increased actin mesh density. They also imply that the greater effect on fertility is due to the late stage effects as opposed to the presence of denser mesh during stage 9. These results are consistent with the hypothesis that Capu and the actin mesh affect fertility and polarity by controlling the timing of cytoplasmic streaming.

CapuNT localizes to the nurse cell cortex and inhibits GFP-CapuΔN

To test whether the effect of GFP-CapuΔN is due to loss of Capu autoinhibition, as opposed to another mechanism such as loss of a binding partner or proper localization of Capu, we expressed GFP-CapuNT (Figure 1A). First we examined GFP-CapuNT's localization in the egg chambers. Previous studies showed that GFP-CapuFL is enriched at the nurse cell cortex, whereas GFP-CapuΔN lacks this localization (Figure 4) [Dahlgaard et al., 2007; Quinlan, 2013]. Therefore, we asked whether the N-terminal half of Capu is sufficient to localize Capu by comparing GFP-CapuNT to GFP-CapuFL. Indeed, GFP-CapuFL and GFP-CapuNT appear similar in the egg chambers: diffuse in both the nurse cell and oocyte cytoplasm, and enriched at the nurse cell cortex (Figure 4). Thus CapuNT is sufficient for localization and the loss of proper localization of GFP-CapuΔN could contribute to misregulation of Capu and the phenotypes we observe. However, we note that the only apparent difference between GFP-CapuΔN and GFP-CapuFL localization is in the nurse cells and no difference in localization is detected in the oocyte.

We also asked whether we could inhibit endogenous Capu in trans by expressing GFP-CapuNT in a wild type background using the *matα* driver. To our surprise, GFP-CapuNT had only a weak effect on fertility compared to *matα*:GFP (63% vs. 73% hatched; Figure 1B). Consistent with the small change we measured in the fertility assay, expression of GFP-CapuNT resulted in a small but significant decrease in actin mesh density at stage 9 when compared to *matα*:GFP oocytes (Figure 2D, J, M and N). However, we note that there was no difference when *matα*:GFP-CapuNT was compared to wild type controls. No change was detected in cytoplasmic streaming (Figure 3D, J, M and N). The fact that this construct does not act as a strong dominant negative suggests that Capu's regulation is more complicated than a single autoregulatory cycle. This is consistent with the fact that Spire and CapuNT bind to the same site within Capu, the Capu-tail [Bor et al., 2012; Vizcarra et al., 2011].

Next, we coexpressed GFP-CapuNT and GFP-CapuΔN in a wild type background using the *matα* driver. Fertility increased from 17% for *matα*:GFP-CapuΔN to 57% when coexpressing GFP-CapuNT and GFP-CapuΔN (Figure 1B). To control for expression strength we also coexpressed GFP with GFP-CapuΔN. This pair resulted in only 27% fertility. Thus GFP-CapuNT can inhibit GFP-CapuΔN in trans, consistent with autoinhibition being a bona fide mode of regulating Capu *in vivo*. We also examined mesh density and cytoplasmic streaming in flies coexpressing GFP-CapuNT and GFP-CapuΔN. The average mesh density in *matα*;GFP-CapuΔN/GFP-CapuNT oocytes was unchanged at stage 9 compared to *matα*;GFP-CapuΔN or *matα*;GFP-CapuΔN/GFP (Figure 2C, E, F, M and Table I). However, densities in oocytes expressing *matα*;GFP-CapuΔN/GFP-CapuNT were broadly distributed at stage 9 compared to *mat*α;GFP-CapuΔN and about half of the oocytes had mesh densities similar to controls. In stage 11 oocytes, the actin mesh density

decreased on average compared to when GFP-CapuΔN was expressed alone or in combination with GFP (Figure 2I, K, L, N and Table I). The average mesh density for *matα*;GFP-CapuΔN/GFP-CapuNT did not recover to wild type levels at stage 11, which is, consistent with the partial recovery of fertility levels (Figure 1B). It is possible that stage 11 oocytes show a larger difference than stage 9 oocytes because they do not have endogenous Capu [Quinlan, 2013]. As expected based on the change in actin mesh, cytoplasmic streaming velocity at stage 11 was higher in *matα*:GFP-Capu-ΔN/GFP-CapuNT oocytes (0.19 μm/s) compared to *matα*:GFP-Capu-ΔN or *matα*:GFP-Capu-ΔN/GFP oocytes (0.04 and 0.09 μm/s respectively) (Figure 3I, K, L, N and Table I). Stage 9 slow streaming was unaffected in these experiments (Figure 3C, E, F, M and Table I).

We also asked whether GFP-CapuNT could modify defects due to GFP-CapuFL overexpression. Consistent with our observation that GFP-CapuNT had little effect when expressed alone, coexpression with GFP-CapuFL did not improve fertility when compared with coexpression of GFP and GFP-CapuFL (54% vs. 59%; Figure 1B). When we expressed GFP-CapuFL in combination with GFP-CapuNT or GFP, mesh density was similar to *matα*;GFP-CapuFL both at stage 9 and 11 (Figure S4A-F, R and Table I). To our surprise, stage 9 actin mesh density was higher for *matα*;GFP-CapuFL/GFP compared to *matα*;GFP-CapuFL and *matα*;GFP-CapuNT/CapuFL. It seems expression of GFP has an effect on the actin mesh. Perhaps GFP weakly activates CapuFL in trans, explaining the increased mesh density we also noted in stage 9 oocytes when GFP alone was expressed (Figure 2). Cytoplasmic streaming in *matα*;GFP-CapuNT/CapuFL oocytes did not differ from GFP-CapuFL expression alone (Figure S4G-Q, S and Table I).

Overall, about half of *matα*:GFP-Capu-ΔN/GFP-CapuNT oocytes had mesh densities and streaming velocities close to wild type, consistent with the fertility rate we measured (57%). Together our data lead us to conclude that, although CapuNT cannot effectively regulate CapuFL in trans, GFP-CapuΔN is more active than GFP-CapuFL because autoinhibition is absent.

Capu impacts mRNA localization during mid-oogenesis

We asked whether unregulated Capu activity disrupts localization of classic polarity factors. To visualize the localization of polarity determinants, we used previously developed live imaging techniques [Becalska and Gavis, 2009]. We coexpressed two transgenes: mRNAs carrying 6-12 copies of the stem-loop binding site for bacteriophage MS2 coat protein (MCP) and MCP protein fused with red fluorescent protein (RFP) or mCherry. MCP binding to the MS2 stem-loop labels the mRNAs in the oocyte. Using this tool, we asked whether the increased actin mesh density at stage 9 or decreased cytoplasmic streaming at stage 11 affected localization of polarity determinants such as *grk*, *osk*, *bcd* and *nanos*. We visualized these mRNAs while expressing GFP, GFP-CapuFL or GFP-CapuΔN using only the *matα* driver because it gives a more pronounced phenotype compared to the *nos* driver.

Early localization of polarity determinants is disrupted by increased Capu activity (Figure 5). Normally, *osk* localizes in a tight band (within 2-3 μm) at the posterior of the oocyte during stages 7-9 [Ephrussi et al., 1991]. We observed diffuse posterior localization of *osk* mRNA (as far as 25 μm away from the posterior) at stage 9 in *matα*:GFP-CapuΔN and

matα:GFP-CapuFL oocytes (Figure 5A-C). By stage 10B, *osk* was more restricted to the posterior for *matα*:GFP-CapuFL but not *matα*:GFP-CapuΔN (Figure 5D-F). It is difficult to distinguish between transport and anchoring defects in this case. The increased mesh density could delay delivery of the *osk* particles. Indeed, the timing correlates with the level of Capu activity. If anchoring is contributing, we do not think this is due to loss of posterior anchoring filaments because these oocytes contain endogenous Capu. Instead the phenotype could reflect an aberrant excess of the anchoring structure. However, we were not able to test this hypothesis due to masking of fine actin structures by the dense and persistent mesh.

In wild type oocytes, *grk* mRNA localizes to the posterior during stages 6-7 and then moves to the anterodorsal corner near the nucleus during stages 9-10 [Jaramillo et al., 2008; Neuman-Silberberg and Schüpbach, 1993]. When we examined *grk*-ms2/MCP-mCherry localization in *matα*:GFP-CapuΔN oocytes during stage 9, we found that most *grk* mRNA localized normally to the anterodorsal corner (Figure S5A, middle row). However, 3 of 15 oocytes had substantially decreased levels of *grk* (Figure S5A, bottom row). In contrast, *grk* was correctly localized in all *matα*:GFP oocytes (12/12). Mislocalization of *grk* leads to disruption of DV axis formation and thereby results in fused dorsal appendages, which we observed in fertility assays [Neuman-Silberberg and Schüpbach, 1993; Schüpbach, 1987]. The low number of dorsalized eggs we observed is consistent with the small fraction of oocytes with mislocalized *grk* mRNA. This low frequency of *grk* mislocalization suggests that perhaps only the highest density of actin mesh at early stages can inhibit the correct localization of *grk*. Even so, the observation is intriguing given that *grk* localization and anchoring are both thought to be solely microtubule dependent.

Both *bcd* and *nanos* localize to the anterior of the oocyte during stages 7-9 [Forrest and Gavis, 2003; Weil et al., 2006]. Their localizations at stage 9 were indistinguishable from wild type in our experiments (Figure S5B, C). Thus despite the fact that fluid dynamics are seemingly unaffected by the denser actin mesh at stage 9 (Figure 3A-C, M), Capu activity has an impact on the early stage of polarity establishment. This effect is not uniform for all mRNAs as *bcd* and *nanos* localization were not affected whereas *osk* and *grk* were.

Capu impacts late phase mRNA localization

Next we examined late stage posterior localization of *nanos* and late stage accumulation of *osk* and *bcd*. Posterior localization of *osk* was normal at stage 13 for both *matα*:GFP-CapuFL and *matα*:GFP-CapuΔN oocytes, indicating that the second phase of *osk* localization is not affected by either the early stage disruption of *osk* localization or the persistence of actin mesh and inhibition of cytoplasmic streaming (Figure 5G-I). This recovery of *osk* localization was surprising given that, normally, late stage transport of *osk* is thought to be driven by cytoplasmic streaming [Glotzer et al., 1997; Sinsimer et al. 2011].

In comparison, the amount of *nanos* at the posterior was low at stage 11 (Figure 5J-N) and stage 13 oocytes (Figure 5O-S). *nanos* localization depends on the correct prior localization of *osk* mRNA and formation of pole plasm [Ephrussi et al., 1991]. Although *osk* localized normally by stage 13, *nanos* levels were low in all stage 11 oocytes (7/7) and most stage 13 oocytes (13/19) expressing *matα*:GFP-CapuΔN (Figure 5J-S). In contrast *matα*:GFP had no effect on *nanos* localization at either stage 11 (6/6) or stage 13 (10/10). We cannot

determine whether the failed *nanos* localization is a direct effect of inhibiting cytoplasmic streaming or a secondary effect of the diffuse posterior localization of *osk* during mid-oogenesis.

bcd localization is normal in *capu* mutants [Manseau et al., 1996]. Interestingly, *bcd* localization to the anterior at late stages of oogenesis was disrupted when Capu activity was increased. Nine of 17 *matα*:GFP-CapuΔN oocytes had no (Figure 5X) or decreased amounts (Figure 5U-W) of *bcd* at the oocyte anterior. In contrast, *bcd* localization was normal in GFP expressing oocytes (10/10) (Figure 5T). We did not detect localization of *bcd* at the posterior of control, matα:GFP-CapuFL or matα:GFP-CapuΔN expressing oocytes (data not shown). These results suggest that an increase in actin mesh density and prevention of cytoplasmic streaming selectively inhibits the second phase of *nanos* and *bcd* mRNA localization but, intriguingly, not that of *osk*. Disruption of *nanos* localization leads to abdominal segmentation defects whereas loss of *bcd* leads to reduced head and thorax [Frohnhofer and Nusslein-Volhard, 1986; Wang and Lehmann, 1991]. These are the phenotypes we observed in our fertility assay (Figure 1C).

Discussion

The role of autoinhibition in regulating Capu

Capu builds an actin mesh in the oocyte during mid-oogenesis (stages 5-10A) in cooperation with Spire [Dahlgaard et al., 2007; Quinlan, 2013]. The two proteins must interact but also spend time apart based on partial-overlapping localization and rescue experiments [Quinlan, 2013]. Thus we hypothesized that Capu is autoinhibited when not associated with Spire. This model led us to expect CapuNT to act as a dominant negative. The fact that it did not behave so suggests that regulation of Capu is more complicated. In fact, CapuNT and Spire bind to the same region of Capu, Capu-tail, and with similar affinities [Bor et al., 2012; Vizcarra et al., 2011]. It follows that competition between the two interactions, in the context of full-length Capu, would lead to autoinhibition dominating. Because the Spire-Capu interaction is necessary, we expect that the oocyte has developed a means of blocking autoinhibition during oogenesis, presumably by reversibly modifying the Capu-tail or the CID. In this case, even excess CapuNT would not have a phenotype. Furthermore, it is possible that localization of GFP-CapuNT confounds its ability to inhibit endogenous function though the major differences in localization between GFP-CapuFL and GFP-CapuNT were in the nurse cells.

We reasoned that GFP-CapuΔN functions free of regulation by Spire after stage 10B because both endogenous Spire and Capu protein levels decrease dramatically at this time [Quinlan, 2013]. Demonstrating that an autoinhibitory interaction can take place in the oocyte, co-expression of GFP-CapuNT with GFP-CapuΔN led to a clear decrease of activity of GFP-CapuΔN at stage 11. Furthermore, this result indicates that the defects due to GFP-CapuΔN expression are largely due to loss of autoinhibition as opposed to loss of another interaction or proper localization.

We conclude that Capu can be autoinhibited in the oocyte and that Capu lacking autoinhibition is deleterious to oocyte development. However, our results suggest that Capu

autoinhibition is a secondary mechanism to regulation by Spire during mid-oogenesis and decreasing Capu protein levels during late oogenesis. Perhaps, Capu functions independently of Spire in other cell types, and Capu autoinhibition plays a more important role there.

Oocyte actin mesh and its role in regulating cytoplasmic streaming

Our data are consistent with the idea that the actin mesh in the oocyte regulates cytoplasmic streaming. Previously, premature streaming had been observed in the absence of actin mesh [Dahlgaard et al., 2007; Theurkauf, 1994]. Complementary to this, we show that a mesh that persists beyond stage 10B is sufficient to inhibit fast streaming. Two outstanding and possibly related questions about the mesh are: What determines mesh density? and How is the mesh removed? Dahlgaard et al. presented evidence that Capu activity level controls mesh density and our data are consistent. We observe that expression of constitutively active Capu increases actin mesh density at both stages 9 and 11 (Figure 2). For GFP-CapuΔN expressing oocytes, we note that the mesh is less dense at stage 11 than 9 (Figure 2 C and I). We do not know what is limiting the actin mesh density at stage 11. This could reflect to the loss of endogenous Spire and Capu [Quinlan, 2013]; limiting amounts of other (unknown) mesh components; the large size of the oocyte at this stage; or the onset of mechanisms to remove the mesh.

Regardless of how mesh density is normally regulated, it can exist at various densities and streaming velocity only loosely correlates with that density (Figure 3). Under wild type conditions, cytoplasmic flows are approximately 30 nm/s during stage 9 and about 10 times faster during stage 11 [Quinlan, 2013]. We note that a two-fold increase in mesh density at stage 11 had minimal effect on streaming, suggesting that streaming can still take place up until some threshold of mesh density. Beyond that, the range of densities and range of streaming velocities we observe suggest that there is a correlation between the two. In contrast, we were intrigued that up to a three-fold (on average) increase in mesh density had no apparent effect on slow streaming at stage 9. We do not know if the rate of mesh turnover is altered by increased Capu activity but normal migration of the nucleus under these conditions suggests that the mesh is not overly stable. If mesh dynamics, i.e. assembly and disassembly, are on the order of the slow fluid flows at stage 9, this would explain why the increased density had no impact.

mRNA transport and localization

Sinsimer et al. [2011] hypothesized that late stage mRNA delivery amplifies the patterns generated earlier in oogenesis. In previous studies of late phase mRNA transport, cytoplasmic streaming was inhibited by depolymerizing the microtubules [Forrest and Gavis, 2003; Glotzer et al., 1997; Weil et al., 2006]. We inhibited cytoplasmic streaming by increasing the actin mesh, enabling us to separate the effects of microtubules and cytoplasmic streaming in late stage transport (Figure 6). The advective transport of cytoplasmic streaming is thought to be responsible for *osk* and *nanos* localization to the posterior during late stages [Forrest and Gavis, 2003; Glotzer et al., 1997; Sinsimer et al., 2011; Snee et al., 2007]. *bcd* also continues to be transported in the late phase but by a mechanism distinct from *osk* and *nanos*. It requires continual active transport mediated by

dynein and microtubules nucleated from the anterior, and depends less on streaming [Weil et al., 2006]. Thus we were surprised to find that *bcd* localization was low or undetectable in about 50% of the egg chambers we examined (Figure 5 and 6). Because transport and anchoring of *bcd* depend on microtubules, the role of streaming could not be separated by colcemid treatment in the original studies of late phase *bcd* localization. The simplest explanation of our results is that streaming plays a greater role than expected. Ooplasmic *bcd* mRNA is dynamic at the anterior. It needs to be continually loaded back on to the microtubules. Perhaps streaming is important for this step, facilitating microtubule/dynein capture events or returning *bcd* that diffused too far away to be captured. Alternatively, Weil et al. [2006] found that the specific subset of microtubules necessary to anchor *bcd* depends on the actin cytoskeleton. Increased Capu activity could alter this arrangement, though we do not favor this explanation, in part because *bcd* localization in *capu* null mutants is normal [Manseau et al., 1996].

Localization of *osk* during early stages (7-10) of oocyte development depends on kinesin and microtubules [Brendza et al., 2000; Ephrussi et al., 1991; Kim-Ha et al., 1991; Parton et al., 2011; Zimyanin et al., 2007]. Continued accumulation of *osk* to the posterior during late stages (11-14) was hypothesized to depend on cytoplasmic streaming [Glotzer et al., 1997; Sinsimer et al., 2011]. We found that inhibiting cytoplasmic streaming by creating a persistent actin mesh does not block transport of *osk* during the second phase of accumulation (Figure 5 and 6). One could interpret this as evidence that streaming is not the transport mechanism. Instead we favor the idea that *osk* (and perhaps multiple mRNAs) are adapted to utilize more than one transport pathway [Sinsimer et al., 2011]. In this case, it is likely that *osk* mRNA is still associated with kinesin during late stages and in the absence of cytoplasmic streaming, *osk* is able to use microtubules, which remain oriented by the persistent mesh, to localize to the posterior. We note that earlier localization of *osk* (stage 9-10B) was not wild type in a manner that corresponded to Capu activity. Instead of a tight strip of posterior localization, we saw partially diffuse *osk* localization at the posterior. The altered localization could be due to defects in the transport and/or anchoring. Perhaps increased Capu activity causes the posterior landing zone to expand, though this would have to be a temporary effect.

The strongest mRNA defect we observed was of late stage *nanos* localization to the posterior. At stage 11, none of the egg chambers had wild type levels of *nanos* and by stage 13, when *osk* was apparently normally localized, only 6 of 19 egg chambers had wild type levels of *nanos* (Figure 5 and 6). While the defect could be secondary, due to the delayed *osk* localization, we believe that inhibiting cytoplasmic streaming is the main cause for this observation. Our data are consistent with those of Forrest and Gavis [2004], who showed that inhibition of cytoplasmic streaming by depolymerization of microtubules results in strongly reduced *nanos* localization. These results together suggest that the primary mechanism for *nanos* localization to the posterior is through the advective forces of cytoplasmic streaming.

Finally, we ask, why does fast cytoplasmic streaming occur? It is counterintuitive to have so much motion in a cell after establishing the localization patterns of crucial polarity factors. Two ideas, which are not mutually exclusive, are: 1) streaming accomplishes long distance

transport in a large cell (diameter of ~100 μm) and 2) streaming is important for mixing the nurse cell cytoplasm with the ooplasm upon dumping. If streaming were the only means of moving mRNAs across the large oocyte, *osk* would not reach the posterior in our experiments. However, *osk* appears to reach the posterior unimpeded by the lack of streaming, demonstrating that streaming is not necessary for long distance transport. Perhaps streaming is a more efficient mode of transport. The modeling and experiments required to test this hypothesis are important future aims. We do not consider *nanos* in this part of the discussion because we cannot distinguish with confidence whether the low posterior localization of *nanos* is due to lack of cytoplasmic streaming or late *osk* delivery. In considering the second idea, we note that lack of mixing between the nurse cell cytoplasm and ooplasm has been observed under conditions that block streaming, e.g. kinesin mutants and increased mesh [Dahlgaard et al., 2007; Palacios and St Johnston, 2002; Serbus et al., 2005; this study]. Why would it be important to mix the cytoplasm if long distance transport were not the reason? Here we can only speculate. We know that gradients of *nanos* and *bicoid* are essential during embryogenesis. We propose that starting with a "clean slate" is a good way to ensure a uniform gradient. Streaming could create a mechanically and chemically clean slate.

Materials and Methods

Molecular Biology

GFP-Capu transgenes were generated by inserting a coding region corresponding to amino acids 1-466 between the BamHI and XbaI sites of pTIGER [Ferguson et al., 2012] with GFP inserted between the KpnI and SpeI sites. Primers were: forward, 5′-ctgttccaggggcccctggg-atccatggccttgcagctaggcaagaag-3′; reverse, 5′-tctactctagatcatttcgtcgaggattggccgca-3′ (Capu1-466). Untagged GFP protein was also inserted in the pTIGER vector.

Drosophila strains

We used the following transgenic fly lines: GFP-CapuFL and CapuFL [Quinlan, 2013], *nos*-GAL4-vp16 [#4937, Bloomington Stock Center, Van Doren et al., 1998], *matα*-GAL4-vp16 [#7063, Bloomington Stock Center, Zimyanin et al., 2007] and hsp83-MCP-RFP [#9940, Bloomington Stock Center, Weil et al., 2006]. GFP-CapuΔN was provided by Daniel St. Johnston [Dahlgaard et al., 2007]. hsp83-MCP-mCherry, *nos*-$(ms2)_6$ and bcd-$(ms2)_6$ were provided by Elizabeth R. Gavis [Forrest and Gavis, 2003; Weil et al., 2006]. *grk*-$(ms2)_{12}$ was provided by Trudi Schüpbach [Jaramillo et al., 2008] and *osk*-$(ms2)_6$ was provided by Tze-Bin Chou [Lin et al., 2008]. CantonS was used as wild type.

Flies expressing each individual Capu construct were assessed for protein levels using quantitative fluorescence imaging (Figure S6). GFP-CapuFL and GFP-CapuΔN were expressed at similar levels at both stages 9 and 11. About twice as much GFP-CapuNT was expressed. Thus the weak phenotypes we observed for this construct were not a result of poor expression.

Fertility assays and abdominal segmentation

Fertility assays were performed as described previously [Quinlan, 2013]. We crossed roughly 100 test females, expressing different Capu proteins in a wild type background, with 40 CantonS males. From these crosses, we quantified the number of hatched eggs as well as the number of eggs that contained fused dorsal appendages [Manseau and Schüpbach, 1989]. Unhatched eggs were collected and prepared for cuticle analysis according to a standard protocol [Alexandre, 2008]. Dark field images were taken using a Zeiss Imager Z.1 equipped with EC Plan-Neofluar 10× 0.3 M27 objective [Edward De Robertis lab, UCLA].

Actin mesh staining and measurement

The oocyte actin mesh was stained as described previously [Quinlan, 2013]. In each experiment, ovaries, which include all stages of development, from 3-4 control (Figures S1A) and 6-8 GFP-Capu expressing flies were dissected and fixed together in 10% paraformaldehyde/PBS. Subsequently, they were stained together using 1 μM AlexaFluor647-phalloidin [Invitrogen] to label actin. We visualized GFP in order to be able to distinguish GFP-expressing egg chamber from control. GFP and AlexaFluor647-phalloidin were excited with 488 and 635 nm lasers, respectively.

Single midsections of oocytes were acquired with a Leica SPE I inverted confocal microscope equipped with an ACS APO 40x/1.15 oil CS immersion objective. Images of control and GFP-Capu-expressing oocytes were acquired with identical conditions. Many times the cortical actin was saturated but care was taken to ensure that the actin mesh was below saturation in our images. To quantify the density of the cytoplasmic actin mesh, the mean intensity of AlexaFluor647-phalloidin was measured in the cytoplasm of WT and GFP-Capu expressing oocytes using Fiji [Schindelin et al., 2012]. To determine the change in actin mesh density, the density of each GFP-Capu expressing oocyte was divided by the average density of 5 control oocytes (Figure S1A). This normalization was performed independently for stage 9 and 11 oocytes, that is, stage 9 controls were collected only for stage 9 experimental oocytes.

Live imaging and cytoplasmic streaming

To trace the movement of the yolk granules (cytoplasmic streaming) or take the single mid-section images of mRNAs (RFP or mCherry), live oocytes were dissected under halocarbon 700 oil and excited with 405 or 532 nm lasers, respectively, using a Leica SPE I inverted confocal microscope. Cytoplasmic streaming data were acquired and analyzed as described previously [Quinlan, 2013] with minor changes. Motion of autofluorescent of yolk granules was determined using particle image velocimetry (PIV) in movies collected every 5 seconds for 2.5 minutes. After the streaming velocities were determined, the speeds of all interrogation windows in a given movie were collated and the 95th percentile speed was reported as a metric for streaming speed to minimize the effects of oocyte geometry and outliers. Sample maximum intensity projections were created in Fiji to show the relative movement of yolk granules [Schindelin et al., 2012].

Statistical analysis of mesh density and cytoplasmic streaming

To compare sets of actin mesh or cytoplasmic streaming data, we determined p-values by applying Student's t-tests. We considered p-values equal to or lower than 0.05 as significantly different. Because some of the data had non-normal distribution, we conducted one-sided Welch's t-tests and Wilcoxon–Mann–Whitney tests. These three analyses returned similar p-values, and therefore supported similar conclusions.

Supplementary Material

Refer to Web version on PubMed Central for supplementary material.

Acknowledgements

We thank the Gavis, Schüpbach and St. Johnston labs for generously sharing fly lines used in our experiments. We thank the De Robertis lab for use of their dark field microscope and the Courey lab for reagents and help with methods. B.B. thanks his parents (Bor Batsuuri and Altanchimeg Mishig) for bringing him to this world and to this country. This work was supported by several funding sources: UCLA Whitcome fellowship (B.B.); National Institutes of Health (R01GM096133), Burroughs-Welcome Fund (Career Award in the Biomedical Sciences), and March of Dimes Foundation (#1-FY12-442) (M.E.Q.). Stocks obtained from the Bloomington Drosophila Stock Center (NIH P4OD018537) were used in this study.

References

Alexandre C. Cuticle preparation of Drosophila embryos and larvae. Methods Mol Biol. 2008; 420:197–205. [PubMed: 18641948]

Becalska AN, Gavis ER. Lighting up mRNA localization in Drosophila oogenesis. Development. 2009; 136:2493–2503. [PubMed: 19592573]

Bor B, Vizcarra CL, Phillips ML, Quinlan ME. Autoinhibition of the formin Cappuccino in the absence of canonical autoinhibitory domains. Mol Biol Cell. 2012; 23:3801–3813. [PubMed: 22875983]

Brendza RP, Serbus LR, Duffy JB, Saxton WM. A function for kinesin I in the posterior transport of oskar mRNA and Staufen protein. Science. 2000; 289:2120–2122. [PubMed: 11000113]

Chang C-W, Nashchekin D, Wheatley L, Irion U, Dahlgaard K, Montague TG, Hall J, Johnston DS. Anterior-Posterior Axis Specification in Drosophila Oocytes: Identification of Novel bicoid and oskar mRNA Localization Factors. Genetics. 2011; 188:883–896. [PubMed: 21625003]

Dahlgaard K, Raposo AASF, Niccoli T, Johnston DS. Capu and Spire assemble a cytoplasmic actin mesh that maintains microtubule organization in the Drosophila oocyte. Dev Cell. 2007; 13:539–53. [PubMed: 17925229]

Emmons S, Phan H, Calley J, Chen W, James B, Manseau L. Cappuccino, a Drosophila maternal effect gene required for polarity of the egg and embryo, is related to the vertebrate limb deformity locus. Genes Dev. 1995; 9:2482–94. [PubMed: 7590229]

Ephrussi A, Dickinson LK, Lehmann R. Oskar organizes the germ plasm and directs localization of the posterior determinant nanos. Cell. 1991; 66:37–50. [PubMed: 2070417]

Ferguson SB, Blundon MA, Klovstad MS, Schüpbach T. Modulation of gurken translation by insulin and TOR signaling in Drosophila. J Cell Sci. 2012; 125:1407–1419. [PubMed: 22328499]

Forrest KM, Gavis ER. Live imaging of endogenous RNA reveals a diffusion and entrapment mechanism for nanos mRNA localization in Drosophila. Curr Biol CB. 2003; 13:1159–1168.

Frohnhöfer HG, Nüsslein-Volhard C. Organization of anterior pattern in the Drosophila embryo by the maternal gene bicoid. Nature. 1986; 324:120–125.

Glotzer JB, Saffrich R, Glotzer M, Ephrussi A. Cytoplasmic flows localize injected oskar RNA in Drosophila oocytes. Curr Biol CB. 1997; 7:326–337.

Gutzeit H. The role of microtubules in the differentiation of ovarian follicles during vitellogenesis in Drosophila. 1986; 195:173–181.

Gutzeit H, Koppa R. Time-lapse film analysis of cytoplasmic streaming during late oogenesis of Drosophila. Development. 1982; 67:101–111.

He B, Doubrovinski K, Polyakov O, Wieschaus E. Apical constriction drives tissue-scale hydrodynamic flow to mediate cell elongation. Nature. 2014; 508:392–396. [PubMed: 24590071]

Higashida C, Miyoshi T, Fujita A, Oceguera-Yanez F, Monypenny J, Andou Y, Narumiya S, Watanabe N. Actin polymerization-driven molecular movement of mDia1 in living cells. Science. 2004; 303:2007–2010. [PubMed: 15044801]

Higgs HN, Peterson KJ. Phylogenetic analysis of the formin homology 2 domain. Mol Biol Cell. 2005; 16:1–13. [PubMed: 15509653]

Hudson AM, Cooley L. Drosophila Kelch functions with Cullin-3 to organize the ring canal actin cytoskeleton. J Cell Biol. 2010; 188:29–37. [PubMed: 20065088]

Jaramillo AM, Weil TT, Goodhouse J, Gavis ER, Schupbach T. The dynamics of fluorescently labeled endogenous gurken mRNA in Drosophila. J Cell Sci. 2008; 121:887–894. [PubMed: 18303053]

Kim-Ha J, Smith JL, Macdonald PM. oskar mRNA is localized to the posterior pole of the Drosophila oocyte. Cell. 1991; 66:23–35. [PubMed: 2070416]

Lehmann R, Nüsslein-Volhard C. Abdominal segmentation, pole cell formation, and embryonic polarity require the localized activity of oskar, a maternal gene in Drosophila. Cell. 1986; 47:141–152. [PubMed: 3093084]

Lehmann R, Nüsslein-Volhard C. The maternal gene nanos has a central role in posterior pattern formation of the Drosophila embryo. Dev Camb Engl. 1991; 112:679–691.

Lin M-D, Jiao X, Grima D, Newbury SF, Kiledjian M, Chou T-B. Drosophila processing bodies in oogenesis. Dev Biol. 2008; 322:276–288. [PubMed: 18708044]

Manseau LJ, Schüpbach T. cappuccino and spire: two unique maternal-effect loci required for both the anteroposterior and dorsoventral patterns of the Drosophila embryo. Genes Dev. 1989; 3:1437–52. [PubMed: 2514120]

Manseau L, Calley J, Phan H. Profilin is required for posterior patterning of the Drosophila oocyte. Development. 1996; 122:2109–16. [PubMed: 8681792]

Neuman-Silberberg FS, Schüpbach T. The Drosophila dorsoventral patterning gene gurken produces a dorsally localized RNA and encodes a TGF alpha-like protein. Cell. 1993; 75:165–174. [PubMed: 7691414]

Otomo T, Tomchick DR, Otomo C, Panchal SC, Machius M, Rosen MK. Structural basis of actin filament nucleation and processive capping by a formin homology 2 domain. Nature. 2005; 433:488–494. [PubMed: 15635372]

Palacios IM, St Johnston D. Kinesin light chain-independent function of the Kinesin heavy chain in cytoplasmic streaming and posterior localisation in the Drosophila oocyte. Dev Camb Engl. 2002; 129:5473–5485.

Parton RM, Hamilton RS, Ball G, Yang L, Cullen CF, Lu W, Ohkura H, Davis I. A PAR-1-dependent orientation gradient of dynamic microtubules directs posterior cargo transport in the Drosophila oocyte. J Cell Biol. 2011; 194:121–135. [PubMed: 21746854]

Paul AS, Paul A, Pollard TD, Pollard T. The role of the FH1 domain and profilin in formin-mediated actin-filament elongation and nucleation. Curr Biol CB. 2008; 18:9–19.

Pruyne D, Evangelista M, Yang C, Bi E, Zigmond S, Bretscher A, Boone C. Role of formins in actin assembly: nucleation and barbed-end association. Science. 2002; 297:612–615. [PubMed: 12052901]

Quinlan ME. Direct interaction between two actin nucleators is required in Drosophila oogenesis. Dev Camb Engl. 2013; 140:4417–4425.

Quinlan ME, Hilgert S, Bedrossian A, Mullins RD, Kerkhoff E. Regulatory interactions between two actin nucleators, Spire and Cappuccino. J Cell Biol. 2007; 179:117–128. [PubMed: 17923532]

Schindelin J, Arganda-Carreras I, Frise E, Kaynig V, Longair M, Pietzsch T, Preibisch S, Rueden C, Saalfeld S, Schmid B, et al. Fiji: an open-source platform for biological-image analysis. Nat Methods. 2012; 9:676–682. [PubMed: 22743772]

Schüpbach T. Germ line and soma cooperate during oogenesis to establish the dorsoventral pattern of egg shell and embryo in Drosophila melanogaster. Cell. 1987; 49:699–707. [PubMed: 3107840]

Serbus LR, Cha B-J, Theurkauf WE, Saxton WM. Dynein and the actin cytoskeleton control kinesin-driven cytoplasmic streaming in Drosophila oocytes. Development. 2005; 132:3743–52. [PubMed: 16077093]

Sinsimer KS, Jain RA, Chatterjee S, Gavis ER. A late phase of germ plasm accumulation during Drosophila oogenesis requires Lost and Rumpelstiltskin. Development. 2011; 138:3431–3440. [PubMed: 21752933]

Snee MJ, Harrison D, Yan N, Macdonald PM. A late phase of Oskar accumulation is crucial for posterior patterning of the Drosophila embryo, and is blocked by ectopic expression of Bruno. Differ Res Biol Divers. 2007; 75:246–255.

Tanaka T, Kato Y, Matsuda K, Hanyu-Nakamura K, Nakamura A. Drosophila Mon2 couples Oskar-induced endocytosis with actin remodeling for cortical anchorage of the germ plasm. Development. 2011; 138:2523–32. [PubMed: 21610029]

Theurkauf W. Premature microtubule-dependent cytoplasmic streaming in cappuccino and spire mutant oocytes. Science. 1994; 265:2093–2096. [PubMed: 8091233]

Theurkauf WE, Smiley S, Wong ML, Alberts BM. Reorganization of the cytoskeleton during Drosophila oogenesis: implications for axis specification and intercellular transport. Dev Camb Engl. 1992; 115:923–936.

Van Doren M, Williamson AL, Lehmann R. Regulation of zygotic gene expression in Drosophila primordial germ cells. Curr Biol CB. 1998; 8:243–246.

Vizcarra CL, Kreutz B, Rodal AA, Toms AV, Lu J, Zheng W, Quinlan ME, Eck MJ. Structure and function of the interacting domains of Spire and Fmn-family formins. Proc Natl Acad Sci. 2011; 108:11884–11889. [PubMed: 21730168]

Wang C, Lehmann R. Nanos is the localized posterior determinant in Drosophila. Cell. 1991; 66:637–647. [PubMed: 1908748]

Wang C, Dickinson LK, Lehmann R. Genetics of nanos localization in Drosophila. Dev Dyn Off Publ Am Assoc Anat. 1994; 199:103–115.

Weil TT, Forrest KM, Gavis ER. Localization of bicoid mRNA in late oocytes is maintained by continual active transport. Dev Cell. 2006; 11:251–262. [PubMed: 16890164]

Zimyanin V, Lowe N, St Johnston D. An oskar-dependent positive feedback loop maintains the polarity of the Drosophila oocyte. Curr Biol CB. 2007; 17:353–359.

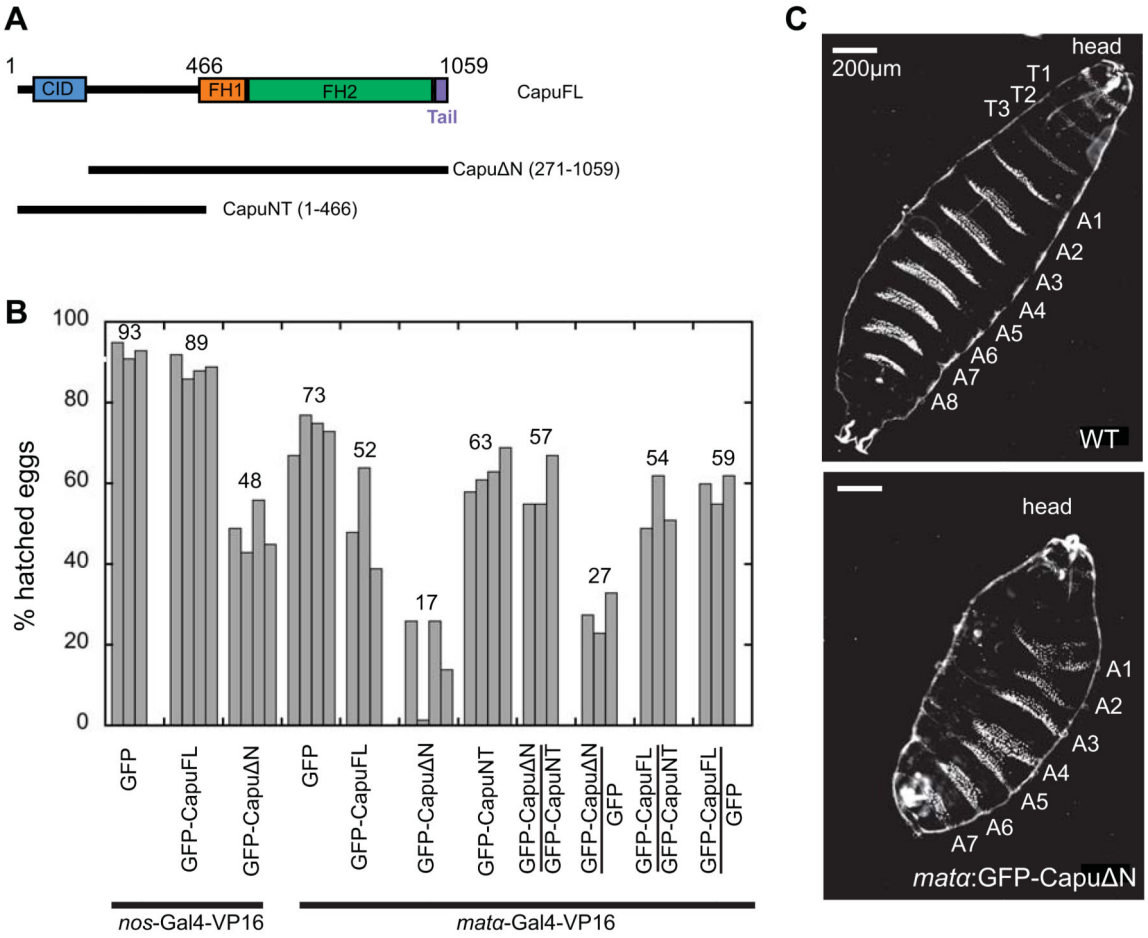

Figure 1. Constitutively active Capu decreases fertility

(A) Domain organization of Capu: CID, Capu Inhibitory Domain (blue); FH1, formin homology 1 domain (orange); FH2, formin homology 2 domain (green); and Capu-tail (violet). Black lines represent constructs used in this study: UASp-GFP (green fluorescent protein)-tagged CapuFL (full-length), CapuΔN and CapuNT. (B) Female fertility represented by % hatched eggs in flies expressing the indicated constructs using either *nos* or *matα* drivers. Each experiment was repeated at least 3 times and is represented by a single bar. The total number of eggs counted is given in Table I. Averages are shown above each group of experiments. (C) Cuticle preparation of embryos derived from wild type (top) or *matα*:GFP-CapuΔN females (bottom). Wild type embryos have 8 abdominal segments (A1-8), 3 thoraces (T1-3) and normal head structure whereas GFP-CapuΔN expressing embryos are abnormally patterned. This cuticle shows only 7 abdominal segments, no thoracic segments and a reduced head structure.

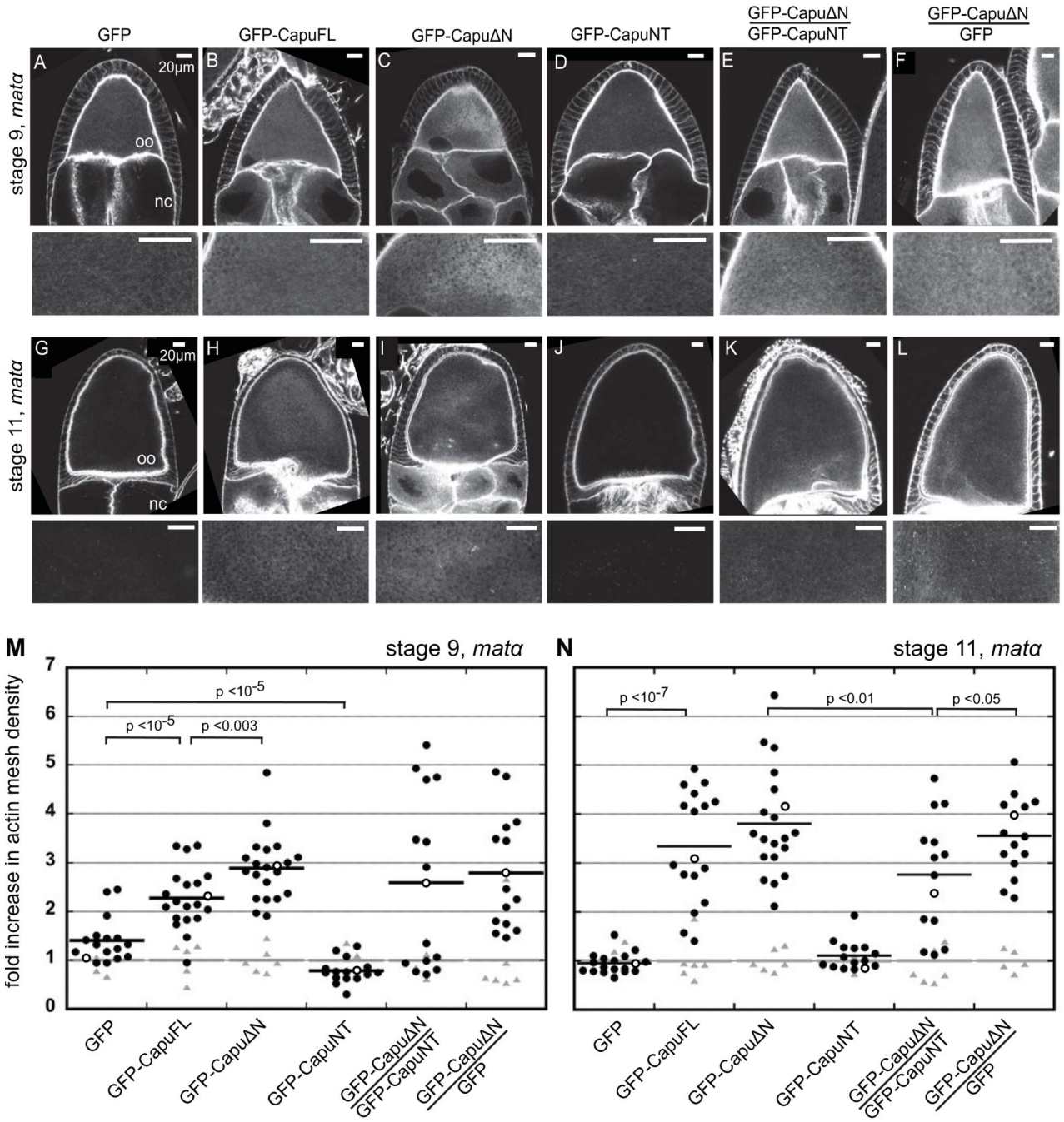

Figure 2. Increased actin mesh density caused by *matα* driven expression of Capu

(A-L) Stage 9 (A-F) and 11 (G-L) egg chambers stained with AlexaFluor647-phalloidin to visualize the actin mesh. In all cases the *matα* driver was used. The constructs expressed are indicated. Images close to the mean intensity (indicated by open circles in the graphs below) were selected for presentation. The lower images are a magnification of the actin mesh in the oocyte. The posteriors of the egg chambers are oriented up. Scale bars are 20 μm. nc, nurse cells: oo, oocytes. (M-N) Dot plots show X-fold increase in oocyte actin mesh density in stage 9 (M) or 11 (N) oocytes (black dots) relative to control oocytes (gray triangles).

Controls were heterozygous for *matα* (Figure S1A). Both control and Capu expressing oocytes were normalized by the average of control oocytes (see methods). Therefore the average of the controls (shown by gray line) is equal to one. The black line represents the mean increase of actin mesh density. p-values were obtained with a Student's t-test (see methods). Only p-values less than or equal to 0.05 are shown.

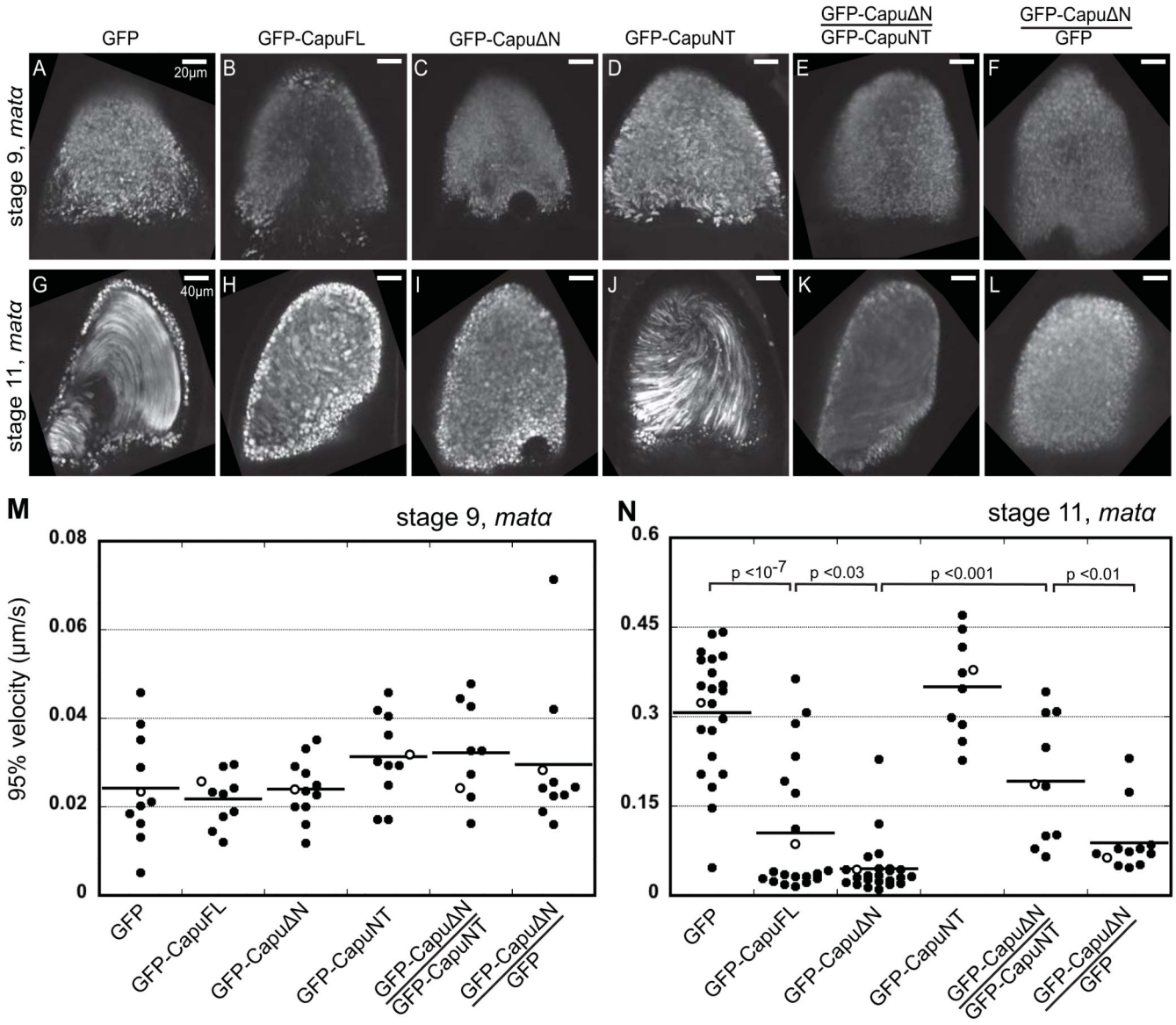

Figure 3. Increased actin mesh density prevents late stage cytoplasmic streaming

Maximum intensity projections of autofluorescent yolk granules for stage 9 (A-F; scale bars are 20 μm) and 11 (G-L, scale bars are 40 μm) oocytes that are expressing different proteins as indicated using the *matα* driver. Each image is representative (shown in open circles in M and N) of 10 or more egg chambers examined. (M, N) Quantification of cytoplasmic streaming using Particle Image Velocimetry (see methods). Dot plots show the 95th percentile of velocities detected. Black lines represent average streaming velocity. p-values were obtained with a Student's t-test (see methods). Only p-values less than or equal to 0.05 are shown.

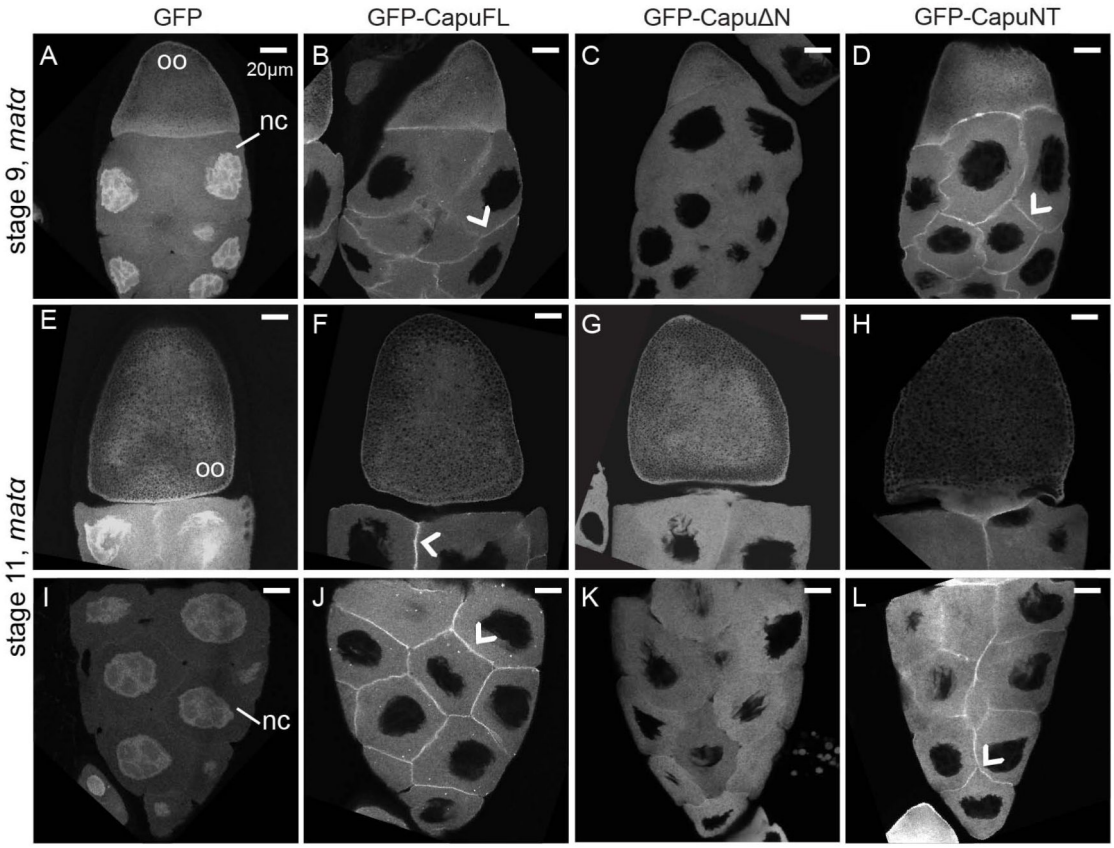

Figure 4. Capu's N-terminus is sufficient to localize Capu

(B, J) Visualization of GFP in fixed eggs shows that GFP-CapuFL localizes to the nurse cell cortex (chevrons) whereas GFP alone (A, I) localizes to the nucleus as well as diffusely in the nurse cells. (C, K) In contrast to full-length Capu, GFP-CapuΔN is not enriched at the nurse cell cortex. (D, L) The N-terminal half of Capu (CapuNT) is sufficient for localization to the nurse cell cortex (chevrons). All proteins had similar diffuse localization in the oocyte (E-H). All scale bars are 20 μm. nc, nurse cells; oo, oocytes.

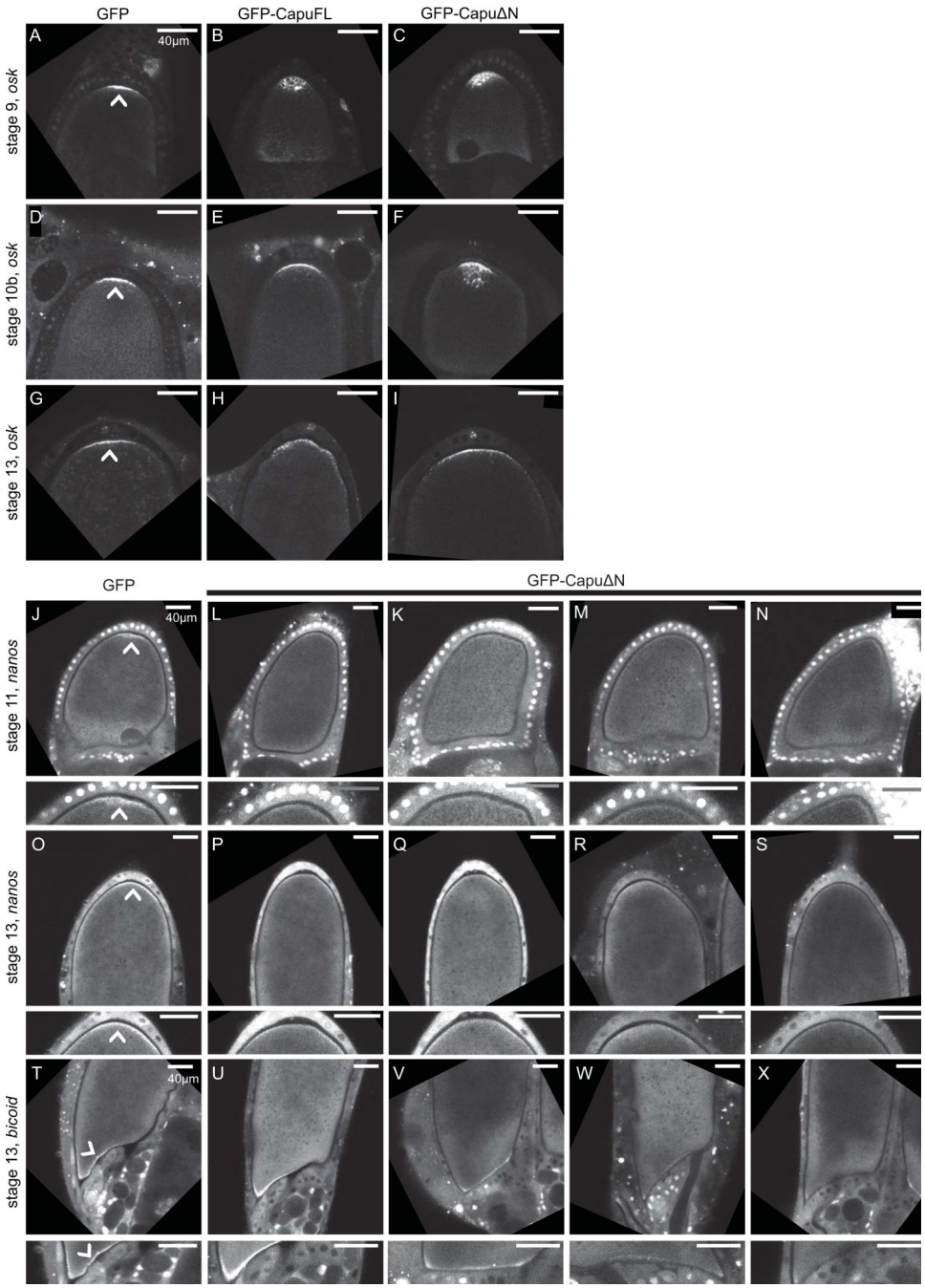

Figure 5. Capu impacts mRNA localization

(A-I) Egg chambers at indicated stages expressing *osk*-(ms2)$_6$ mRNA and MCP-RFP in combination with *matα*:GFP, *matα*:GFP-CapuFL or *matα*:GFP-CapuΔN. *osk* accumulates at the posterior forming a narrow band at all stages in controls (A, D, G, chevrons). In contrast, *osk* has a diffuse posterior localization in stage 9 *matα*:GFP-CapuFL and *matα*:GFP-CapuΔN oocytes (B, C). By stage 10B localization is more restricted in *matα*:GFP-CapuFL but not *matα*:GFP-CapuΔN oocytes (E, F). By stage 13, *osk* is restricted to a tight band in the posterior; experimental flies are indistinguishable from control flies (G-I). (J-X) Egg

chambers expressing MCP-mCherry and *nanos*-$(ms2)_{18}$ (J-S) or *bcd*-$(ms2)_6$ (T-X) in combination with either *matα*:GFP or *matα*:GFP-CapuΔN. The lower images are 3x magnifications of the posterior for *nanos* and anterior for *bcd. nanos* (in stage 11 and 13) and *bcd* (stage 13 only) localized to the posterior and anterior similar to wild type *osk* mRNA in GFP expressing oocytes (J, O, T, chevrons). Multiple images showing the expression pattern (high to low from left to right) of the *nanos* (L-N, P-S) or *bcd* (U-X) in *matα*:GFP-CapuΔN oocytes. All scale bars are 40 μm.

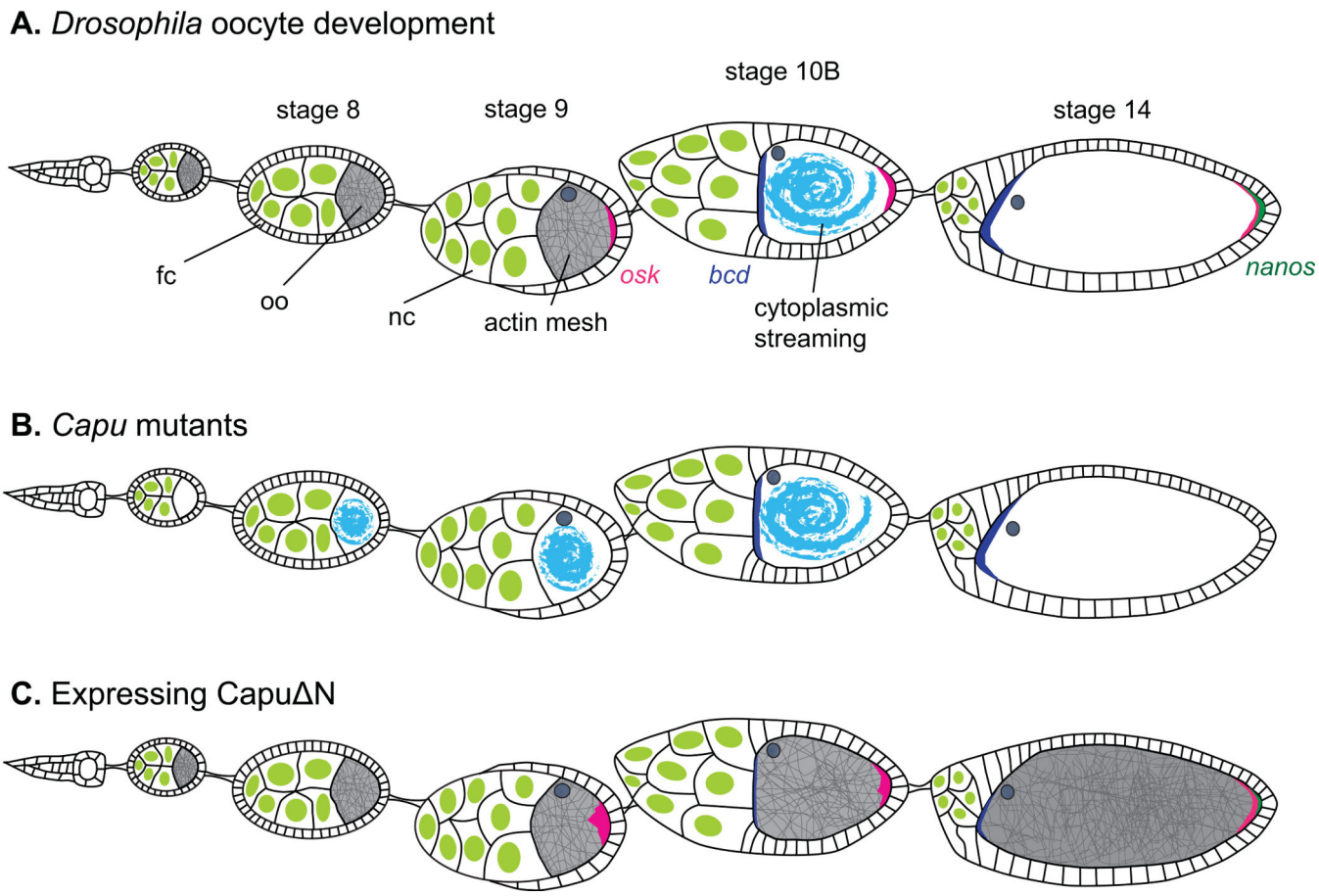

Figure 6. *Drosophila* oocyte development in wild type, *capu* mutant and constitutively active Capu expressing oocytes

The posterior of the oocytes are oriented to the right. (A) Wild type oocytes (oo) are surrounded by follicle cells (fc) and have an actin mesh from early stages to stage 9. During stage 10, the actin mesh (grey) disappears and fast cytoplasmic streaming (blue) begins. Shortly after streaming begins, nurse cells (nc) dump their contents into the oocyte, resulting in expansion of oocytes during late stages. *Oskar* (*osk*, pink) mRNA localizes to the posterior region from early stages (7-9) and is enriched through stage 14. *Bicoid* (*bcd*, blue) mRNA localizes to the anterior region of the oocyte from late stage 10 to stage 14. *Nanos* (green) mRNA localizes to the posterior of the oocytes during late stages in an *osk* dependent manner. (B) In *capu* null mutants, the actin mesh is absent and cytoplasmic streaming begins prematurely. Both *osk* and *nanos* localizations are disrupted in the mutant oocytes whereas *bcd* localization is wild type. (C) Expression of constitutively active Capu (CapuΔN) resulted in denser actin mesh at early stages and persistent mesh at stages 10-14. Fast cytoplasmic streaming was inhibited during late stages. In this case, *osk* was not tightly localized to the posterior at stage 9 or 10B but was normally localized later. Both anterior localization of *bcd* and posterior localization of *nanos* were decreased or completely disrupted.

Table I

Change in actin mesh, cytoplasmic streaming and egg fertility.

driver	fly genotypes	% Hatched[a]	Stage 9, average fold increase in actin mesh	Stage 11, average fold increase in actin mesh	Stage 9, average cytoplasmic streaming (μm/s)	Stage 11, average cytoplasmic streaming (μm/s)
nos	GFP	93 (n=450)	1.0	1.1	0.03	0.29
	GFP-CapuFL	89 (493)	1.8	1.8	0.03	0.29
	GFP-CapuΔN	48 (772)	2.2	2.5	0.03	0.15
	GFP-CapuNT	97 (580)	ND	ND	ND	ND
matα	GFP	73 (799)	1.4	0.9	0.02	0.31
	GFP-CapuFL	52 (910)	2.3	3.3	0.02	0.11
	GFP-CapuΔN	17 (613)	2.9	3.8	0.02	0.04
	GFP-CapuNT	63 (313)	0.8	1.1	0.03	0.35
matα	GFP-CapuΔN / GFP-CapuNT	55 (600)	2.6	2.8	0.03	0.19
	GFP-CapuΔN / GFP	25 (600)	2.8	3.6	0.02	0.09
matα	GFP-CapuFL / GFP-CapuNT	53 (525)	2.5	3.0	0.03	0.08
	GFP-CapuFL / GFP	58 (437)	3.3	2.8	0.02	0.1

ND, not determined.

[a] percent of eggs hatched in at least 3 independent experiments. n = total number of eggs.